

K. SARAVANAKUMAR^{1*}, J. NAMPOOTHIRI¹, M.R. PRATHEESH KUMAR¹

WIRE ARC ADDITIVE MANUFACTURING OF ALUMINIUM 5356 ALLOY: PROCESS PARAMETER OPTIMIZATION AND STRUCTURE-PROPERTY ANALYSIS

Wire Arc Additive Manufacturing (WAAM) is an emerging technology in the manufacturing sector, offering benefits such as increased production rates and cost efficiency. This study investigates the WAAM of aluminium alloy 5356, deposited on aluminium 6082 base plates. Key process parameters – arc current, stick-out distance, and travel speed – were optimized using an L9 orthogonal array to improve the quality of multi-wall structures. The optimized parameters facilitated the construction of multi-wall structures using a zig-zag pattern. Microstructural and mechanical properties were analyzed using scanning electron microscopy, tensile testing, and Vickers hardness testing. The results revealed significant differences in grain structure, with coarse grains in the top region and finer grains in the bottom, influenced by varying solidification rates. Additionally, the optimized parameters reduced the occurrence of cracks and pores.

Keywords: WAAM; GMAW; L9 orthogonal array; aspect ratio; zig-zag pattern

1. Introduction

Wire Arc Additive Manufacturing (WAAM) is a promising technology for the efficient and cost-effective production of large, complex metal parts [1]. WAAM utilizes an electric arc as the heat source and continuous wire as the feedstock material, depositing successive layers to create three-dimensional structures [1]. This technique offers several advantages, including efficient material utilization, faster build speeds, and flexibility in working with a wide range of metal alloys, making it particularly suitable for industries such as aerospace, automotive, energy, and marine [1,2].

Recent research has focused on optimizing WAAM processes to improve dimensional precision and surface finish, further enhancing its viability as a cost-effective production method [3,4]. Studies have also examined microstructural properties and hardness of single-track thin walls manufactured using gas metal arc welding (GMAW) at various welding speeds and heat inputs [5]. These investigations revealed preferred crystallographic planes, textured structures, and variations in α -Al + Si formations, contributing to the continuous optimization of the WAAM process [6]. Beyond process optimization, material development has gained significant attention, particularly in the biomedical and automotive sectors. For instance, β -titanium

alloys, designed to mimic human bone properties, are widely used in the biomedical field, while titanium alloys are favoured in aerospace and automotive applications for their lightweight properties [7]. Among additive manufacturing techniques, selective laser melting and electron beam melting have emerged as the most effective methods for achieving full densification and high dimensional accuracy in 3D-printed titanium and its alloys [8].

In recent literature, path planning strategies have also been explored to improve the dimensional accuracy and overall performance of printed parts [9]. These strategies are particularly beneficial for components with complex shapes and intricate structures, showcasing their adaptability in meeting diverse design requirements [10]. One such strategy is the zig-zag deposition pattern, which has been reported as effective in improving the uniformity of layer deposition and reducing residual stresses in some additive manufacturing processes [11-13]. While the zig-zag pattern has shown promise in areas like laser-based additive manufacturing, its effectiveness has not yet been extensively explored for WAAM, particularly in the deposition of aluminium alloys such as Al 5356.

To advance WAAM's capability in fabricating intricate parts with wire structures, a robotic approach has been proposed, involving optimization of welding parameters through bead modeling and collision-free path planning. This method has

¹ DEPARTMENT OF PRODUCTION ENGINEERING, PSG COLLEGE OF TECHNOLOGY, COIMBATORE, TAMIL NADU 641 004, INDIA

* Corresponding author: ksk.prod@psgtech.ac.in



successfully enabled the fabrication of complex wire structures, demonstrating its effectiveness and feasibility [14]. WAAM has also been investigated for repairing corroded structures, such as using the Cold Metal Transfer (CMT) process to deposit aluminium filler material ER4043 on AA5052 in marine environments [15]. Microstructural analysis revealed that the CMT + Pulse mode produces fine-grain structures, and the corrosion resistance of WAAM-repaired parts is comparable to that of wrought components, further highlighting its industrial potential [16].

Despite these advancements, several challenges persist in WAAM applications, such as high heat input leading to residual stresses, undesirable microstructures, and phase transformations [17]. Ancillary processes like post-processing heat treatments, stress-relief annealing, and advanced in-situ monitoring systems have been explored to improve WAAM part quality [18]. Post-processing heat treatments, such as annealing, help relieve residual stresses by allowing the material to thermally relax, redistributing internal stresses, and refining the microstructure [19-21]. Stress-relief annealing, in particular, involves heating components below their melting point, followed by controlled cooling to reduce residual stresses [21-23]. Additionally, advanced in-situ monitoring systems provide real-time insights into temperature distribution and stress states, enabling dynamic adjustments to welding parameters, minimizing residual stress formation while maintaining desired microstructural characteristics [19-23].

However, further research on aluminium 5356 alloys fabricated using the zig-zag strategy is required, particularly to understand the properties and microstructural features across multi-wall layer structures. Therefore, this study aims to optimize gas metal arc welding (GMAW) parameters for the deposition of Al 5356 filler wire on Al 6082 base plates. Using an L9 orthogonal array, this research investigates the influence of process parameters on the microstructural and mechanical properties of multi-wall structures. The objective is to minimize defects such as cracks and pores while enhancing the overall quality and performance of WAAM processes.

2. Materials and methods

Aluminium 5356 alloy was used as the filler wire material, selected for its high strength and corrosion resistance. A 1.2 mm diameter electrode was employed for preparing weld beads and multi-wall layered structure on a base plate. The baseplate material chosen was Aluminium 6082, with dimensions of 30 mm×150 mm×15 mm. To ensure a successful welding process, Gas Metal Arc Welding (GMAW) was selected, known for its oxide cleaning effect, which reduces hydrogen content in the oxidation layer and minimizes warpage.

The compositions of both alloys were verified through Energy Dispersive Spectroscopy (EDS) tests, as shown in Fig. 1. For the WAAM trials, the parameters selected were arc current, electrode stick-out distance, and travel speed, with 100% argon gas supplied at a rate of 15 liters per minute [24]. The arc current directly influences heat input, and its careful selection ensures proper fusion without overheating, preventing potential defects. The stick-out distance affects droplet transfer stability and heat distribution, and its optimization is crucial for maintaining uniformity in the molten pool. The travel speed impacts bead width and cooling rates, and adjusting it helps control the thermal distortion, ensuring the desired bead geometry [25-26]. Therefore, these parameters were selected for optimization due to their significant impact on deposition quality and mechanical properties. The specific levels for each parameter are provided in TABLE 1.

TABLE 1

Parameters and their levels for WAAM trials using Al 5356 filler wire on Al 6082 base plates

S. No	Parameters	Levels		
		I	II	III
1	Arc-current (A)	80	100	120
2	Stick-outdistance (mm)	10	12	14
3	Travelspeed (mm/s)	3	4	5

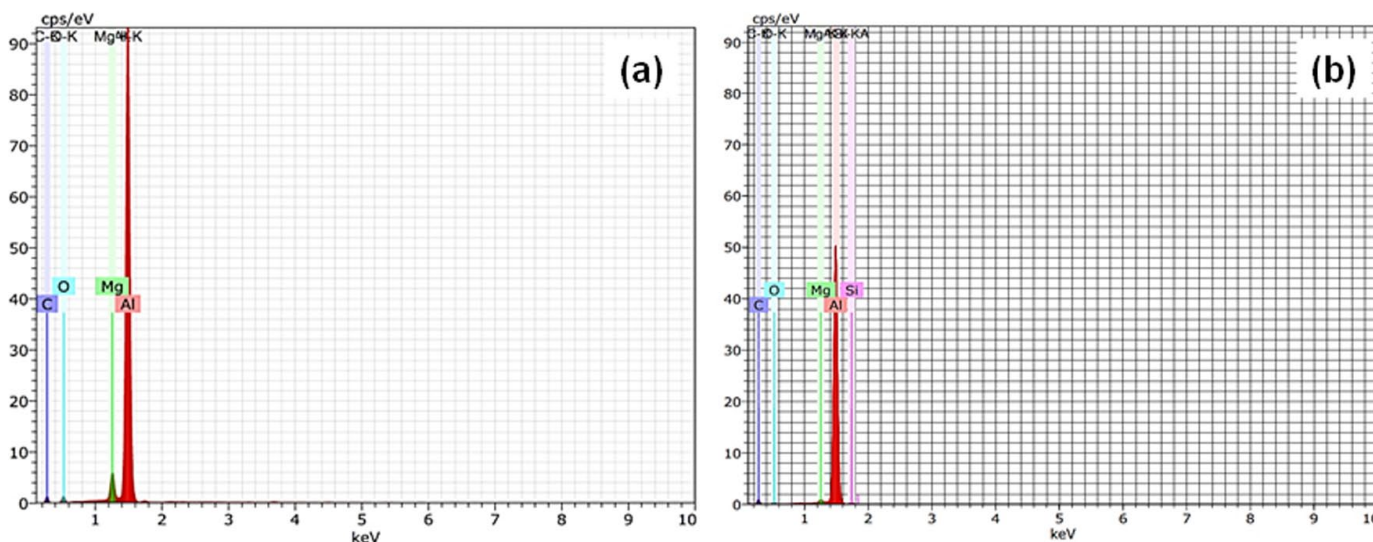


Fig. 1. Energy Dispersive Spectroscopy pattern of a) Al 5356 filler wire and b) Al 6082 base plates for composition analysis

An L9 orthogonal array is a Latinized experimental design matrix used for experiments involving multiple factors. Typically, an L9 orthogonal array involves three factors, each with three levels, resulting in 9 experimental runs, detailed in TABLE 2.

The GMAW welding unit with FANUC robotic arm used for the multi wall structure preparations is shown in Fig. 2(a) and

characteristic features of the bead such as arc radius and height was measured using a coordinate measuring machine (Mitutoyo crysta apex – S544, Japan), as depicted in Fig. 2(b). For optimization, an L9 orthogonal array was employed to explore parameter interactions, and ANOVA for an alpha value of 0.05 (TABLE 4) was used to identify significant factors influencing the aspect ratio (ratio of weld bead height to its width for WAAM [12]), followed by Excel Solver for parameter optimization to achieve the highest aspect ratio.

Following each layer deposition using the optimized parameters during the WAAM trials, a dwell time of 120 seconds was implemented to ensure even cooling between layers, thereby mitigating defects such as porosity and cracks. This dwell time was chosen based on preliminary trials, which highlighted the importance of balancing thermal conditions during the build process. The 120-second interval allowed for sufficient heat dissipation between layers, preventing excessive thermal gradients that could lead to warping, cracks, or porosity. The prepared multi-wall layer of dimensions 150×130×20 mm is depicted in Fig. 3.

TABLE 2

Design of Experiments [18]

Exp. No	Current (A)	Stickout Distance (mm)	Travel Speed (mm/s)
1	80	10	3
2	100	10	4
3	120	10	5
4	80	12	4
5	100	12	5
6	120	12	3
7	80	14	5
8	100	14	3
9	120	14	4

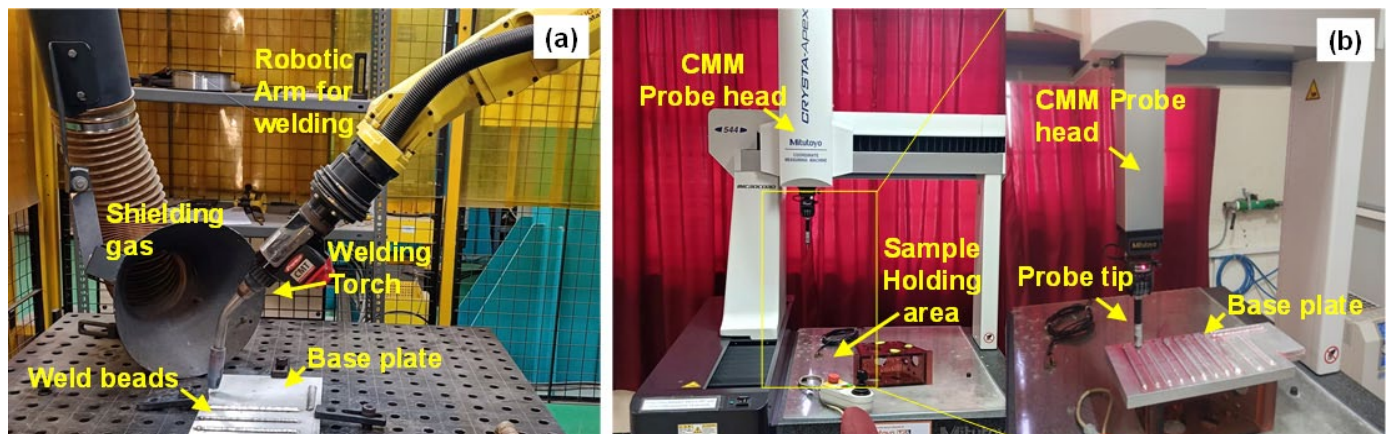


Fig. 2. Images of (a) the equipment used for multi wall structure development and (b) coordinate measuring machine

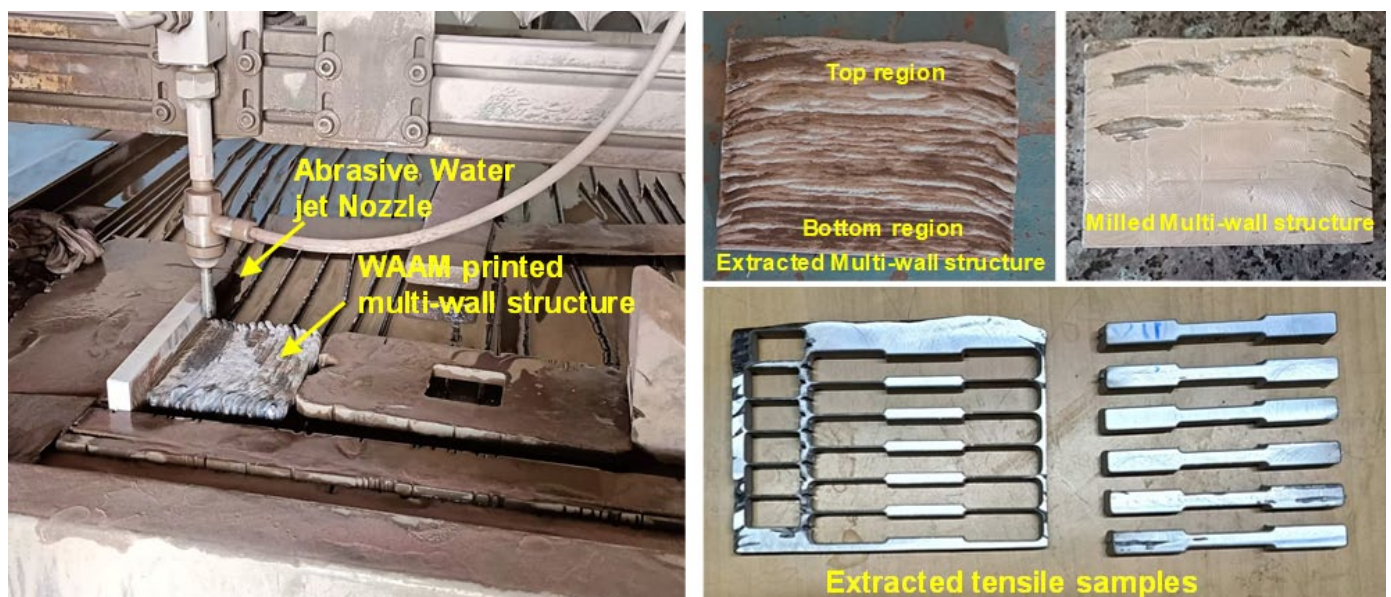


Fig. 3. Sample extraction from the multilayer wall structure using abrasive waterjet machining

Samples were extracted from the prepared multilayer wall structure for microstructure analysis, microhardness testing, and tensile testing using abrasive waterjet machining, depicted in Fig. 3. The microstructure samples were polished using standard metallography procedures and analyzed using the Carl Zeiss Evo 18 Scanning Electron Microscope. Vickers microhardness was measured at a load of 0.2 kg with a dwell time of 10 seconds. Tensile tests were performed in accordance with ASTM E8 standards, employing a gauge length of 32 mm.

To study the properties of the aluminium 5356 alloy, the tensile samples was cut from the top to bottom layer of the multiwall structure as shown in the Fig. 3.

3. Results and discussion

Optimization identifies the optimal combination of input variables to achieve desired process outputs, focusing on achieving the best bead quality in terms of height and width. This involves analyzing key parameters influencing the process and using aspect ratios to determine optimal parameter values.

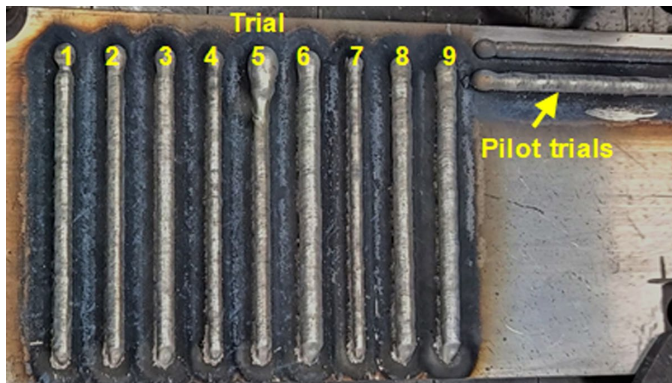


Fig. 4. Weld beads prepared for optimization of WAAM parameters

From the data gathered from weld bead samples shown in Fig. 4, and tabulated in the TABLE 3, it can be inferred that the aspect ratio is better in sixth sample when compared to other samples.

The results of the design of experiments are given in TABLE 3 where the aspect ratio of sixth bead is larger (1.787) when compared to the other sample's aspect ratio. When the aspect ratio is larger, then it means the width and height of bead will be larger. Using process parameters of sixth bead, a multiwall structure was built using GMAW process.

TABLE 3

Design of experiments with aspect ratio

Sample No	Current (A)	Stickout distance (mm)	Travel speed (mm/s)	Height (mm)	Width (mm)	Aspect ratio
1	80	10	3	5.466	6.735	1.232
2	100	10	4	4.907	6.755	1.376
3	120	10	5	4.215	7.253	1.330
4	80	12	4	4.885	6.373	1.305
5	100	12	5	3.77	6.564	1.741
6	120	12	3	5.45	9.199	1.787
7	80	14	5	3.643	5.108	1.402
8	100	14	3	5.325	8.249	1.549
9	120	14	4	0.5	0.8	1.772

The ANOVA presented in TABLE 4 estimates that the all the 3 parameters and their interactions are significant in determining the aspect ratio of the weld bead. The interaction term has a p-value of 0.00011, which is significantly less than 0.05, indicating that the interaction between the factors (arc current, stickout distance, and travel speed) also significantly affects the response variables. Also, the F-value (10.89) exceeds the F-critical value (2.93), suggesting that the combined influence of the factors should be considered.

Fig. 5 illustrates microstructure samples from the top and bottom regions of the multiwall structure. Gas metal arc welding (GMAW) influences cooling rates, affecting heat accumulation due to the presence of current. The lower base plate temperatures cause immediate solidification of the melt pool, resulting in porosity formation in the lower regions (Fig. 5(a)), which indicates hydrogen presence from the additive manufacturing process. The porosity primarily originates from hydrogen absorbed from both the atmosphere and the filler wire during the welding process [27]. Hydrogen, which is trapped during solidification, contributes to pore formation due to its reduced solubility in solid aluminium [28]. As the multiwall structure height increases, heat accumulation and solidification rates vary, affecting the porosity distribution and grain structure [29,30]. This results in the top portion of the structure being relatively defect-free (Fig. 5(b)), as the cooling rate is more controlled, allowing for more uniform solidification. In addition to the porosity observed, traces of hot cracks were found in the bottom region, closer to the base plate. These hot cracks may be a result of the rapid cooling near the base plate, where the thermal gradient is more significant, causing solidification stresses and leading to crack formation.

TABLE 4

ANOVA for the parameters and response

ANOVA						
Source of Variation	SS	df	MS	F	P-value	F crit
Sample	9.099605556	2	4.549803	13.16294	0.0003	3.554557
Columns	541.5520027	2	270.776	783.3766	3.15E-18	3.554557
Interaction	15.05921111	4	3.764803	10.89187	0.000115	2.927744
Within	6.221743333	18	0.345652			
Total	571.9325627	26				

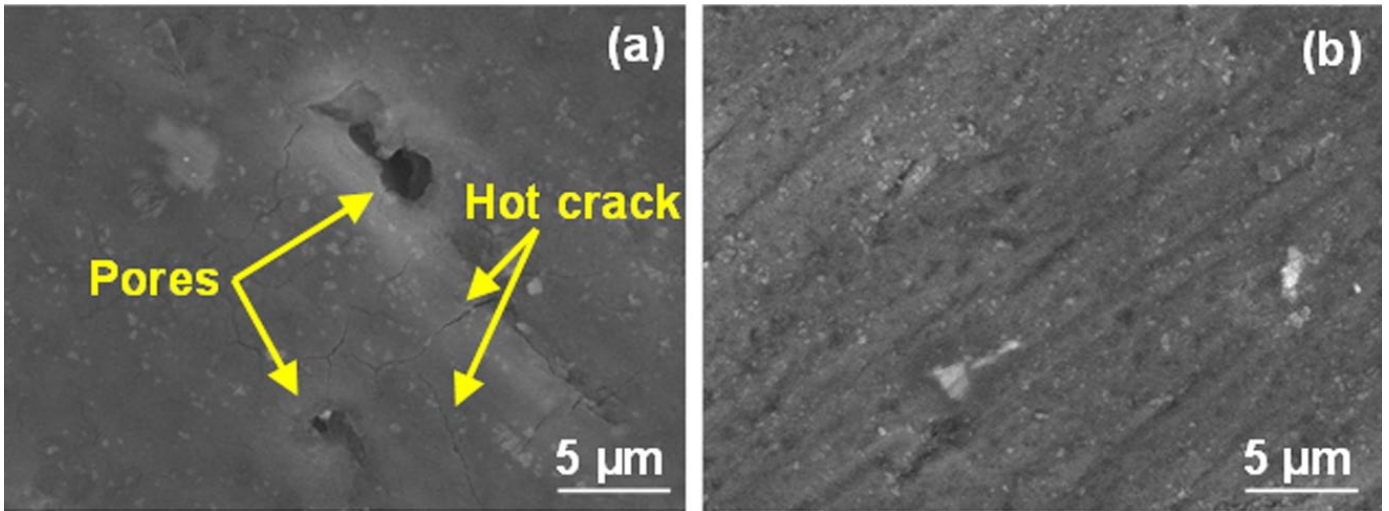


Fig. 5. Microstructure Analysis of WAAM printed multi-wall structure from (a) bottom region and (b) top region

Microhardness testing offers valuable insights into material properties such as ductility, toughness, and strength at a microstructural level. In this study, microhardness tests conducted on the top and bottom regions of the multiwall structure revealed a gradual decrease in hardness from the bottom (highest hardness of 74 HV) to the top as shown in Fig. 6, which is indicative of heat accumulation between layers during the build-up of the multiwall structure. This trend is influenced by the solidification rates and microstructural refinement occurring during the WAAM process. The performance characteristics of aluminum alloy parts produced using WAAM are strongly influenced by critical input factors such as travel speed, stickout distance, and arc current [30].

Higher travel speeds typically result in rapid solidification, promoting the formation of finer microstructures and potentially increasing microhardness due to the enhanced cooling rates [30]. In contrast, lower travel speeds allow for more heat input, leading to slower cooling rates, which can result in coarser

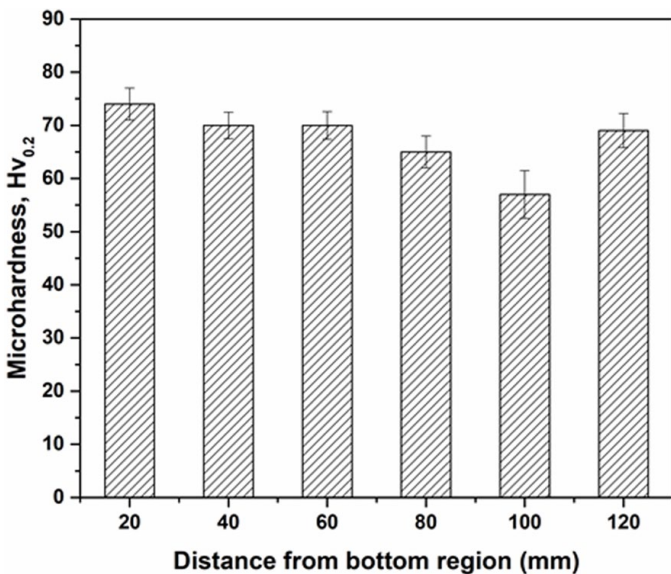


Fig. 6. Microhardness of multilayer wall structure

microstructures and a reduction in microhardness [30]. Longer stickout distances tend to increase heat input because of the higher electrical resistance, which can lead to increased microhardness. However, if the stickout distance becomes excessive, it can destabilize the arc, causing inconsistent heat distribution and irregularities in the microstructure, which may negatively affect the resulting microhardness [30]. Similarly, higher welding currents increase heat input, which promotes faster melting and deeper penetration, potentially resulting in higher microhardness by improving the material's ability to resist deformation.

The ultimate tensile strength in this study ranges from 203.342 MPa to 249.429 MPa as shown in Fig. 7, indicating a notable influence of grain size and pore distribution on mechanical properties. Notably, the ultimate tensile strength increased to 249.429 MPa at a reduced travel speed of 180 mm/min compared to 241.7 MPa at 320 mm/min reported by Tawfik et al. [31]. The zig-zag pattern implementation further enhances ultimate tensile strength, even at lower travel speeds. Fine grains

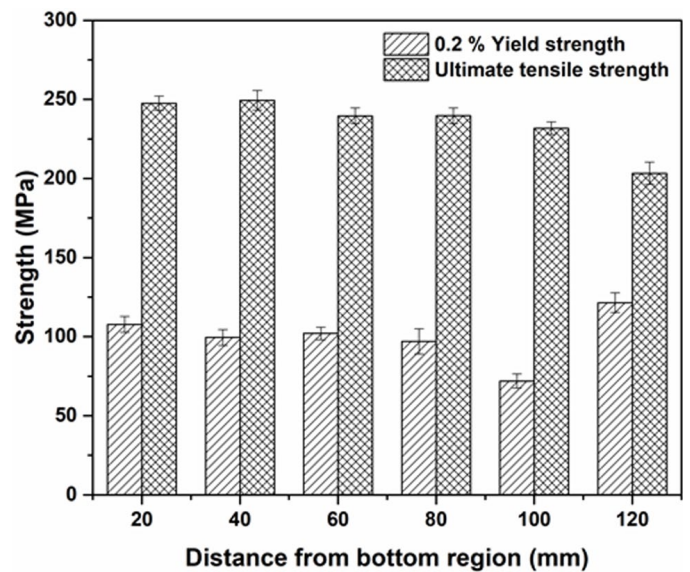


Fig. 7. Tensile properties of the multiwall structure

at the bottom region exhibit superior tensile properties due to effective grain boundary hindrance against crack propagation, while coarse grains at the bottom show reduced tensile properties due to significant pore impact on grain boundaries. The microstructural analysis reveals that higher porosity and larger internal grain sizes significantly influence mechanical properties, with hydrogen pores acting as stress concentrators that promote localized stress and initiate crack formation and propagation. Regions with larger grain sizes are particularly vulnerable to these effects due to fewer grain boundaries impeding pore influence. Conversely, smaller grain sizes exhibit increased grain boundary density, more effectively hindering crack propagation and contributing to higher tensile strength, attributed to the Hall-Petch effect [22]. This effect impedes dislocation movement in smaller grains, making crack propagation more challenging.

Fractography analysis was conducted to elucidate the fracture characteristics and underlying causes of material failure. Examination of fracture surfaces via SEM images identified fracture modes and factors such as material defects, manufacturing flaws, and loading conditions contributing to failure. In this study, SEM images of fractured areas from the upper and lower regions of the multi-wall structure revealed small pores and cracks in the top samples (Fig. 8(a&b)), with slight dimple formations indicative of ductile fracture [32]. Dimple features were more prominent than pores in both upper and lower regions, suggesting dominant ductile characteristics in the multi-wall structure. Fractographic analysis revealed that both the top and bottom portions displayed minor dimples indicative of ductile fracture. However, secondary cracks were observed within the dimples at the bottom, where pores acted as stress concentrators, initiating and propagating cracks. In contrast, no porosity was observed in the top portion. This variation in porosity influenced the mechanical properties of the multi-wall structure. The multi-wall structure, fabricated using a zig-zag pattern with aluminium 5356 alloy, exhibited ductile characteristics as evidenced by the SEM images. Pores observed within the dimples contributed to crack initiation and propagation, reducing load-carrying capacity and plasticity [31].

4. Conclusion

In this study, gas metal arc welding (GMAW) with aluminium 5356 filler wire and aluminium 6082 base plate was utilized to create a multi-wall structure, evaluated through an L9 orthogonal array of weld beads, with an arc current of 120 A, stick-off distance of 12 mm and a travel speed of 3 mm/s found to be optimal for best aspect ratio. Microstructural analysis revealed coarse grains predominantly in the upper regions and finer grains in the lower regions of the multi-wall structure, corresponding with solidification rates and the entrapment of hydrogen during the welding process. The microhardness results showed 74 HV_{0.2} at the bottom region and a 65 HV_{0.2} in the top region, with smaller grain sizes enhancing microhardness due to increased grain boundaries that obstruct dislocation movement. The maximum ultimate tensile strength was found to be 249.429 MPa, with fine grains at the bottom exhibiting superior tensile properties compared to the coarse grains at the top. Fractography revealed minor dimples indicative of ductile fracture on the bottom, and with secondary cracks observed within dimples where pores were present, acting as stress concentrators that initiate and propagate cracks in the bottom, ultimately influencing the mechanical properties of the multi-wall structure.

Acknowledgement

The authors sincerely thank the Management, PSG College of Technology, Coimbatore, Tamil Nadu for their support and provision of facilities.

REFERENCES

- [1] R. Rumman, D.A. Lewis, J.Y. Hascoet, J.S. Quinton, Laser metal deposition and wire arc additive manufacturing of materials: An overview. *Arch. Metall. Mater.* **64** (2), 467-473 (2019). DOI: <https://doi.org/10.24425/amm.2019.127561>

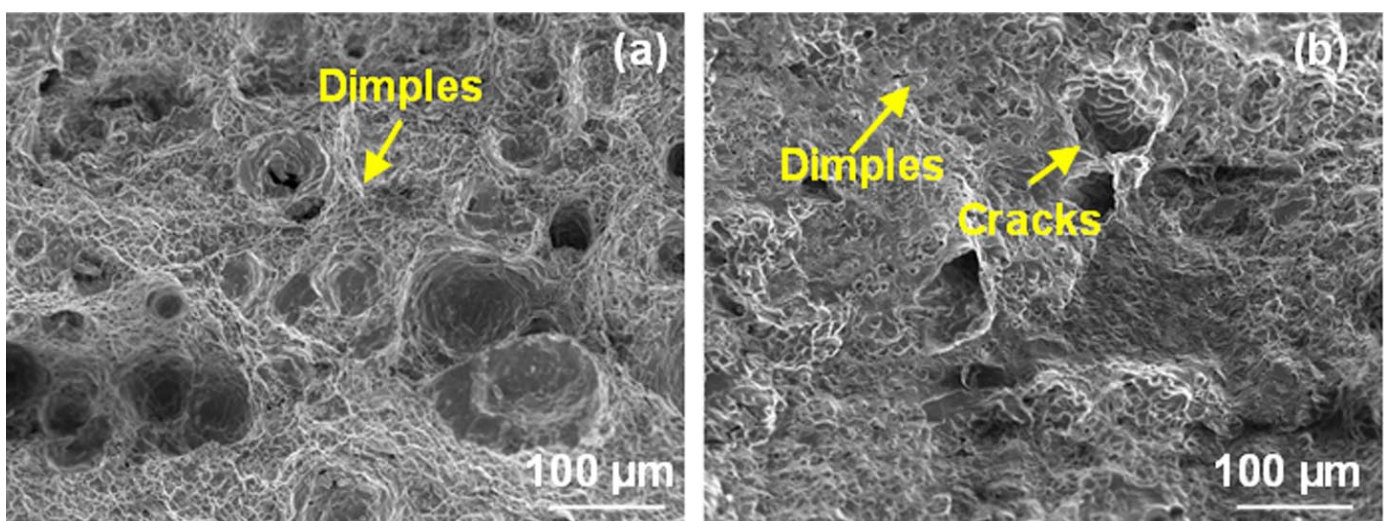


Fig. 8. SEM images of fractured areas from the multi-wall structure. (a) bottom region and (b) top region

- [2] K.S. Derekar, A review of wire arc additive manufacturing and advances in wire arc additive manufacturing of aluminium. *Materials Science and Technology* **34** (8), 895-916 (2018).
DOI: <https://doi.org/10.1080/02670836.2018.1455012>
- [3] Z. Wang, X. Lin, L. Wang, Y. Cao, Y. Zhou, W. Huang, Microstructure evolution and mechanical properties of the wire + arc additive manufacturing Al-Cu alloy. *Addit. Manuf.* **47**, 102298 (2021).
DOI: <https://doi.org/10.1016/j.addma.2021.102298>
- [4] D. Jafari, T.H.J. Vaneker, I. Gibson, Wire and arc additive manufacturing: Opportunities and challenges to control the quality and accuracy of manufactured parts. *Mater. Des.* **202**, 109471 (2021).
DOI: <https://doi.org/10.1016/j.matdes.2021.109471>
- [5] S.W. Williams, F. Martina, A.C. Addison, J. Ding, G. Pardal, P. Colegrove, Wire + Arc Additive Manufacturing. *Mater. Sci. Technol.* **32** (7), 641-647 (2015).
DOI: <https://doi.org/10.1179/1743284715Y.0000000073>
- [6] J. Ge, S. Pillay, H. Ning, Post-process treatments for additive-manufactured metallic structures: A comprehensive review. *J. Mater. Eng. Perform.* **32**, 7073-7122 (2023).
DOI: <https://doi.org/10.1007/s11665-023-08051-9>
- [7] D.J. Kim, H.G. Kim, J.S. Kim, K.H. Song, Properties of pure Ti implants fabricated by additive manufacturing. *Arch. Metall. Mater.* **64** (3), (2019).
DOI: <https://doi.org/10.24425/amm.2019.129480>
- [8] H.J. Rack, J.I. Qazi, Titanium alloys for biomedical applications. *Mater. Sci. Eng. C* **26** (8), 1269-1277 (2006).
DOI: <https://doi.org/10.1016/j.msec.2005.08.032>
- [9] N. Singh, P. Hameed, R. Ummethala, G. Manivasagam, K.G. Prashanth, J. Eckert, Selective laser manufacturing of Ti-based alloys and composites: impact of process parameters, application trends, and future prospects. *Mater. Today Adv.* **8**, 100097 (2020).
DOI: <https://doi.org/10.1016/j.mtadv.2020.100097>
- [10] M.S.M. Mansor, S. Raja, F. Yusof, M.R. Muhamad, Y.H.P. Manurung, M.S. Adenan, N.I.S. Hussein, J. Ren, Integrated approach to Wire Arc Additive Manufacturing (WAAM) optimization: Harnessing the synergy of process parameters and deposition strategies. *J. Mater. Res. Technol.* **30**, 2478-2499 (2024).
DOI: <https://doi.org/10.1016/j.jmrt.2024.03.170>
- [11] W. Hackenhaar, J.A.E. Mazzaferro, C.C.P. Mazzaferro, et al., Effects of different WAAM current deposition modes on the mechanical properties of AISI H13 tool steel. *Weld World* **66**, 2259-2269 (2022).
DOI: <https://doi.org/10.1007/s40194-022-01342-0>
- [12] J. Müller, J. Hensel, WAAM of structural components – building strategies for varying wall thicknesses. *Weld World* **67**, 833-844 (2023). DOI: <https://doi.org/10.1007/s40194-023-01481-y>
- [13] M.H. Ali, Y.S. Han, Effect of Phase Transformations on Scanning Strategy in WAAM Fabrication. *Materials* **14**, 7871 (2021).
DOI: <https://doi.org/10.3390/ma14247871>
- [14] Q. Wang, J. Jia, Y. Zhao, A. Wu, In situ measurement of full-field deformation for arc-based directed energy deposition via digital image correlation technology. *Addit. Manuf.* **72**, 103635 (2023).
DOI: <https://doi.org/10.1016/j.addma.2023.103635>
- [15] G. Ma, G. Zhao, Z. Li, et al., Optimization strategies for robotic additive and subtractive manufacturing of large and high thin-walled aluminum structures. *Int. J. Adv. Manuf. Technol.* **101**, 1275-1292 (2019).
DOI: <https://doi.org/10.1007/s00170-018-3009-3>
- [16] M. Vishnukumar, R. Pramod, A. Rajesh Kannan, Wire arc additive manufacturing for repairing aluminium structures in marine applications. *Mater. Lett.* **299**, 130112 (2021).
DOI: <https://doi.org/10.1016/j.matlet.2021.130112>
- [17] S. Kesarwani, N. Yuvaraj, M.S. Niranjana, CMT-based WAAM: a comprehensive review of process parameters, their effects, challenges, and future scope. *J. Braz. Soc. Mech. Sci. Eng.* **46**, 699 (2024).
DOI: <https://doi.org/10.1007/s40430-024-05276-0>
- [18] Q. Wu, T. Mukherjee, A. De, T. DebRoy, Residual stresses in wire-arc additive manufacturing – Hierarchy of influential variables. *Additive Manufacturing* **35**, 101355 (2020).
DOI: <https://doi.org/10.1016/j.addma.2020.101355>
- [19] F.D. Gurmesa, H.G. Lemu, Y.W. Adugna, M.D. Harsibo, Residual Stresses in Wire Arc Additive Manufacturing Products and Their Measurement Techniques: A Systematic Review. *Applied Mechanics* **5**, 420-449 (2024).
DOI: <https://doi.org/10.3390/applmech5030025>
- [20] K. Wandtke, D. Schroepfer, R. Scharf-Wildenhain, et al., Influence of the WAAM process and design aspects on residual stresses in high-strength structural steels. *Weld World* **67**, 987-996 (2023).
DOI: <https://doi.org/10.1007/s40194-023-01503-9>
- [21] N.A. Rosli, M.R. Alkahari, M.F. Abdollah, S. Maidin, F.R. Ramli, S.G. Herawan, Review on effect of heat input for wire arc additive manufacturing process. *J. Mater. Res. Technol.* **11**, 2127-2145 (2021). DOI: <https://doi.org/10.1016/j.jmrt.2021.02.002>
- [22] B. Parvaresh, H. Aliyari, R. Miresmaeili, et al., Ancillary processes for high-quality additive manufacturing: A review of microstructure and mechanical properties improvement. *Met. Mater. Int.* **29**, 3103-3135 (2023).
DOI: <https://doi.org/10.1007/s12540-023-01444-4>
- [23] L.P. Raut, R.V. Taiwade, Wire Arc Additive Manufacturing: A comprehensive review and research directions. *J. Mater. Eng. Perform.* **30**, 4768-4791 (2021).
DOI: <https://doi.org/10.1007/s11665-021-05871-5>
- [24] K. Saravanakumar, S. Ananth, J. Medoline, M. Dharshini, K.M. Sansuuki Priyanka, Investigation of microstructure and mechanical properties of Aluminium 5356 using Wire Arc Additive Manufacturing. *J. Adv. Mech. Sci.* **2** (3), 82-98 (2024).
DOI: <https://doi.org/10.5281/zenodo.10523562>
- [25] A. Queguineur, R. Asadi, M. Ostolaza, et al., Wire arc additive manufacturing of thin and thick walls made of duplex stainless steel. *Int. J. Adv. Manuf. Technol.* **127**, 381-400 (2023).
DOI: <https://doi.org/10.1007/s00170-023-11560-5>
- [26] A. Voropaev, R. Korsmik, I. Tsubulskiy, Features of filler wire melting and transferring in wire-arc additive manufacturing of metal workpieces. *Materials* **14**, 5077 (2021).
DOI: <https://doi.org/10.3390/ma14175077>
- [27] P. Jiangang, Y. Bo, G. Jinguo, R. Yu, C. Hongjun, Z. Liang, L. Hao, Influence of arc mode on the microstructure and mechanical

- properties of 5356 aluminum alloy fabricated by wire arc additive manufacturing. *J. Mater. Res. Technol.* **20**, 1893-1907 (2022). DOI: <https://doi.org/10.1016/j.jmrt.2022.08.005>
- [28] M. El-Shennawy, H.A. Abdel-Aleem, M.M. Ghanem, et al., Effect of welding parameters on microstructure and mechanical properties of dissimilar AISI 304/ductile cast iron fusion welded joints. *Scientific Reports* **14** (1), 19827 (2024). DOI: <https://doi.org/10.1038/s41598-024-70050-0>
- [29] N. Chernovol, F. Marefat, B. Lauwers, et al., Effect of welding parameters on microstructure and mechanical properties of mild steel components produced by WAAM. *Weld World* **67** (6), 1021-1036 (2023). DOI: <https://doi.org/10.1007/s40194-022-01422-1>
- [30] B. Turgut, U. Gürol, R. Onler, Effect of interlayer dwell time on output quality in wire arc additive manufacturing of low carbon low alloy steel components. *International Journal of Advanced Manufacturing Technology* **126** (11), 5277-5288 (2023). DOI: <https://doi.org/10.1007/s00170-023-11481-3>
- [31] M.M. Tawfik, M.M. Nemat-Alla, M.M. Dewidar, Effect of travel speed on the properties of Al-Mg aluminum alloy fabricated by wire arc additive manufacturing. *J. Mater. Eng. Perform.* **30**, 7762-7769 (2021). DOI: <https://doi.org/10.1007/s11665-021-05959-y>
- [32] C. Su, X. Chen, C. Gao, Y. Wang, Effect of heat input on microstructure and mechanical properties of Al-Mg alloys fabricated by WAAM. *Appl. Surf. Sci.* **486**, 431-440 (2019). DOI: <https://doi.org/10.1016/j.apsusc.2019.04.255>